Materials Today Physics 16 (2021) 100305

Contents lists available at ScienceDirect

Materials Today Physics

journal homepage: https://www.journals.elsevier.com/materials-today-physics

Phonon weak couplings model and its applications: A revisit to two-temperature non-equilibrium transport

Chengcheng Deng [a], Yuwen Huang [a, b], Meng An [c], Nuo Yang [a, b, *]

[a] School of Energy and Power Engineering, Huazhong University of Science and Technology, Wuhan, 430074, PR China
[b] State Key Laboratory of Coal Combustion, Huazhong University of Science and Technology, Wuhan, 430074, PR China
[c] College of Mechanical and Electrical Engineering, Shaanxi University of Science and Technology, Xi'an, 710021, PR China

ARTICLE INFO

Article history:
Received 26 August 2020
Received in revised form
12 October 2020
Accepted 13 October 2020
Available online 20 October 2020

Keywords:
Nanoscale
Thermal transport
Low-dimensional materials
Van der Waals cross-interfaces
Two-temperature model

ABSTRACT

The thermal management on low-dimensional materials requires a fundamental understanding of phonon couplings, which dominates thermal transport. In this mini-review, recent studies on weak couplings between phonon and other energy carriers are reviewed firstly. Then, a generalized analytical model, phonon weak couplings model, is proposed based on Boltzmann transport equation. When applying this model to describe recent works on weak couplings of phonons, it is classified as "implicit couplings" and "explicit couplings", corresponding to couplings within a single structure and between two structures, respectively. Furthermore, perspectives and limitations of phonon weak couplings model are summarized, and potential research prospects are given to inspire future investigations and applications.

1. Introduction

Modern electronic devices are aggressively shrinking into nanoscale and operate with increasing volumetric power consumption, thermal management in devices becomes a critical issue in current advanced technology [1]. There is an increasing demand for materials with high thermal conductivity and interfacial thermal conductance that can dissipate massive heat in electronic devices [2–7]. Because phonons play a critical role in the thermal transport in micro/nanoscale semiconductors, phononics and phonon engineering have drawn lots of attentions [8–12]. Therefore, a fundamental and comprehensive understanding of phonon transport mechanism is crucial to improve the performance of materials and devices for effective thermal management.

Extensive studies show that two main thermal resistances play central roles in determining the thermal conductivity of materials. The first one is the phonon coupling thermal resistance between different phonon groups inside low-dimensional materials, which determine the thermal conductivity of single material itself [13]. The second one is the interfacial thermal resistance between different structures or materials, which determine the total thermal conductivity of composite materials [14,15]. A very important feature in such systems is the coupled thermal transport among different phonon groups or thermal channels. Coupled thermal transport phenomena are observed to exist in many applications including thermal management, thermal modulation, thermoelectrics and energy conversion, such as phonon transport in low-dimensional materials with high thermal conductivity like graphene [16] and boron nitride nanoribbons [17], heat transfer across metal-dielectric interfaces [18], heat conduction in folded graphene for phononic device [19], and water evaporation with nanoparticles for solar desalination [20,21].

Totally different from strong couplings among phonons in bulk structures, it is found recently that there are much weaker couplings in nanostructures, which play an important role in dominating the thermal properties of nanomaterials. The finding of phonon-phonon weak coupling is important which is related to some new physical phenomena such as two-temperature non-equilibrium thermal transport and hot topic such as van der Waals interfaces. For example, the weak coupling between in-plane phonons and out-of-plane phonons in the suspended graphene resulted in the non-equilibrium thermal transport, which is one of the central factors for the high thermal conductivity of graphene [22]. Besides, the widespread van der Waals interfaces between

* Corresponding author. School of Energy and Power Engineering, Huazhong University of Science and Technology, Wuhan, 430074, PR China.
E-mail address: nuo@hust.edu.cn (N. Yang).

https://doi.org/10.1016/j.mtphys.2020.100305
2542-5293/

nanostructures are featured with weak interactions [23–25], which also exhibit similar phonon-phonon weak coupling between two interacting subsystems. Therefore, there is a great demand for a generalized theoretical model to reveal the physical mechanism for coupled thermal transport phenomena in a systematic way.

In this work, firstly, the related studies of coupling between phonon and other energy carriers, such as electron-phonon and magnon-phonon, are reviewed. Then, the necessity of model to describe phonon-phonon coupling is illustrated. In part 3, phonon weak couplings model (PWCM) is deduced based on Boltzmann transport equation. In part 4, when applying PWCM to describe the mechanism of phonon weak couplings in thermal transport, it is classified in two situations. One is "implicit couplings" between different phonon groups/branches within one single structure, and the other is "explicit couplings" across the interface between two different structures. Finally, perspectives, limitations and prospects of PWCM are given.

2. Coupling between phonon and other energy carriers

The coupling between phonon and other energy carriers, which takes non-negligible effects on thermal transport, has been investigated recently. Two different types of energy carriers, such as the electron-phonon or magnon-phonon, can be easily driven into non-equilibrium state through their different interactions with external excitations or different boundary conditions [26]. One approach to conveniently investigate the coupling is the two-temperature model (TTM) [27,28], where two types of energy carriers are considered as two subsystems with coupling interaction. It is named as two-temperature because the temperature profiles of two subsystems usually deviate from each other due to non-equilibriums. Generally, the interaction between subsystems is much weaker than that within each subsystem. The interacting degree between subsystems is described by a coupling factor.

Take an example of electron-phonon coupling, the governing equations of two subsystems by TTM are:

$$C_e\frac{\partial T_e}{\partial t}=\nabla(k_e\nabla T_e)-G_{ep}(T_e-T_p) \tag{2-1a}$$

$$C_p\frac{\partial T_p}{\partial t}=\nabla(k_p\nabla T_p)+G_{ep}(T_e-T_p) \tag{2-1b}$$

where e and p refer to electron and phonon respectively, T is the temperature while t is time, C is the volumetric heat capacity of the energy carriers, and G_{ep} is the e-p coupling factor.

The observation of electron-phonon local non-equilibrium dates back to decades ago during experiments on laser excitation of crystalline metals [29]. While the direct measurement of energy carriers' temperature is difficult, researchers turn to theoretical models in predicting and interpreting experimental results. Majumdar and Reddy used TTM to show that electron-phonon coupling could be an important issue in metal-nonmetal interfaces [28]. Chen adopted TTM to predict a large non-equilibrium between electrons and phonons created at a properly designed potential step which can produce a large thermoelectric effect [30].

Fig. 1 shows the representative temperature profiles derived from TTM at a metal-dielectric interface. Electron-phonon coupling causes the two temperature profiles to deviate from each other near the interface, resulting in the so-called e-p non-equilibrium phenomenon. This presents a total temperature jump including the temperature difference related to the electron-phonon coupling in the metal side and the phonon-phonon coupling across the interface. Through the combination of two-temperature model and molecular dynamics, a method named TTM-MD is

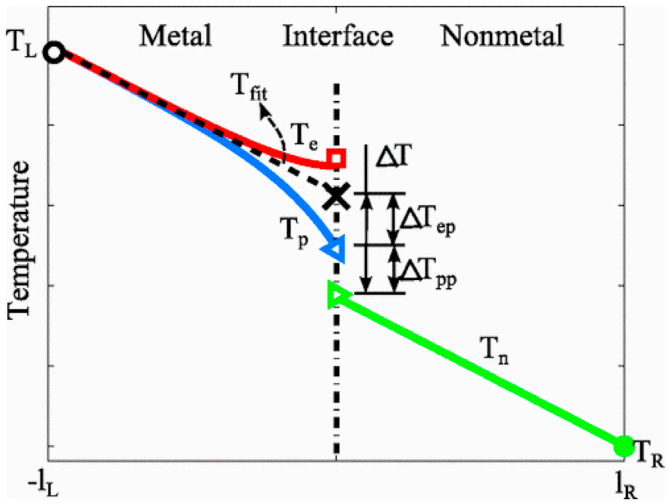

Fig. 1. Representative temperature profiles in TTM for electron-phonon coupling across metal-nonmetal interface from Ref. [32]. In the metal side near interface, electrons and phonons have different temperatures (T_e and T_p) indicating the non-equilibrium transport caused by electron-phonon coupling. The total temperature difference at the interface (ΔT) is denoted by the sum of temperature difference induced by electron-phonon coupling in the metal side (ΔT_{ep}) and temperature difference induced by phonon-phonon coupling across the interface (ΔT_{pp}). Reprinted with permission from Ref. [32]. Copyright (2012) American Physical Society.

developed to effectively simulate electron-phonon coupling in both metal [31] and metal/semiconductor interface [32]. The basic idea of TTM-MD is to represent electrons' scattering with phonons as a "friction force" added to the atoms in the simulation domain. TTM-MD was then modified by including the cross-interface electron-phonon coupling [33]. Moreover, TTM was extended to a general multi-temperature model (MTM), by calculating the e-ph scattering rates from first principles and then solving their coupled transport in conjunction with ph-ph scattering rates, which account for the phonon branch-resolved electron-phonon coupling [34,35]. In addition, thermal modulation can be achieved from the perspective of electron-phonon coupling, such as an appropriate choice of interlayer materials with relatively strong electron-phonon coupling could significantly enhance interfacial thermal transport across metal-dielectric interfaces [36], and the critical particle size could be identified to enhance thermal conductivity of metal nanoparticle-polymer composites [37].

For the magnon-phonon coupling, TTM has been successfully applied to study thermally driven spin transport and energy conversion phenomena. Sanders and Walton [27] used TTM to treat the coupled phonon-magnon thermal diffusion process, where magnons and phonons were modeled as two gases of bosons with different temperatures but each locally in thermal equilibrium. TTM was also applied to explain the spin Seebeck effect [38], and was further extended to take into account the boundary heat and spin transfer [39]. Liao et al. generalized TTM for coupled phonon-magnon diffusion to include the effect of the concurrent magnetization flow, and predict a new magnon cooling effect driven by a nonuniform magnetic field [40]. Recently, An et al. has reported the experiments in which the local non-equilibrium between magnons and phonons was found in a single crystalline bulk magnetic insulator, and the diffusion length of thermal magnons was quantified through analyzing the deviation in the magnon number density from the local equilibrium value [41].

According to previous studies, it can be seen that two-temperature model is applicable to describe the coupling between phonon and other types of energy carriers, such as electron-

phonon and magnon-phonon. Generally, the interaction between different types of carriers is much weaker than that among the same type of carriers. The coupling interaction between the same type of energy carriers (such as phonon-phonon coupling) mainly present strong coupling in the materials. Recently, it is found that weak coupling also exists between phonon and phonon [22,42,43]. From the perspective of coupling strength, it is necessary to propose a special model to describe the composite couplings of phonon-phonon for different situations, such as phonon coupling between two subsystems including two different phonon groups/branches or two different structures/materials.

From the definition of temperature, TTM is applicable to describe two different temperatures of two types of energy carriers at the same location. That is, TTM does not include the situations that different temperatures in different structures with couplings, such as van der Waals interfaces. From different perspectives of analysis, TTM is named from the introduction of physical parameter "temperature" under the framework of non-equilibrium transport. In contrast, here we focuses more on the strength of coupling among different phonons and the underlying physical mechanism. Therefore, a generalized model named as phonon weak couplings model is proposed to give a clear physical description of coupling mechanism, and this model is applied to summarize recent works including both the "implicit couplings" and "explicit couplings" under the framework of phonon coupling.

3. Derivation of phonon weak couplings model

In the phonon weak couplings model, the coupling effects can be considered between two interacting subsystems, such as two different phonon groups/branches or two different structures/materials. It is noteworthy that the phonon transport in separate subsystem is much stronger than that between the two subsystems. But the phonon coupling between the two subsystems still has inescapable impact on the thermal transport in the entire system. The theoretical derivation of PWCM in such systems is given as follows.

It is assumed that the interaction between two subsystems is so weak that the coupling has a negligible effect on the distribution and phase space of phonons in each subsystem. Therefore, the phonon distribution functions (f) in two subsystems can be separately determined by the Boltzmann transport equation (BTE) as follows:

$$\frac{\partial f_1}{\partial t}+\mathbf{F}\cdot\nabla_{\mathbf{p}}f_1+\mathbf{v}\cdot\nabla_{\mathbf{r}}f_1=\left(\frac{\partial f_1}{\partial t}\right)_c \tag{3-1a}$$

$$\frac{\partial f_2}{\partial t}+\mathbf{F}\cdot\nabla_{\mathbf{p}}f_2+\mathbf{v}\cdot\nabla_{\mathbf{r}}f_2=\left(\frac{\partial f_2}{\partial t}\right)_c \tag{3-1b}$$

where the subscripts *1* and *2* denote the phonons in two subsystems, respectively. When the system reaches steady state without applying external force, the Eq. (3-1a) and Eq. (3-1b) can be simplified as:

$$\mathbf{v}\cdot\nabla_{\mathbf{r}}f_1=\left(\frac{\partial f_1}{\partial t}\right)_c \tag{3-2a}$$

$$\mathbf{v}\cdot\nabla_{\mathbf{r}}f_2=\left(\frac{\partial f_2}{\partial t}\right)_c \tag{3-2b}$$

where the right-hand side is the collision term in each subsystem, which includes both the scatterings inside subsystem itself and the scatterings between two subsystems. Thus, the Eq. (3-2a) and Eq. (3-2b) can be written as:

$$\mathbf{v}\cdot\nabla_{\mathbf{r}}f_1=\left(\frac{\partial f_1}{\partial t}\right)_{11}+\left(\frac{\partial f_1}{\partial t}\right)_{12} \tag{3-3a}$$

$$\mathbf{v}\cdot\nabla_{\mathbf{r}}f_2=\left(\frac{\partial f_2}{\partial t}\right)_{22}+\left(\frac{\partial f_2}{\partial t}\right)_{12} \tag{3-3b}$$

where the subscript *11*, *22*, *12* respectively denote the phonon scatterings inside the first subsystem, the phonon scatterings inside the second subsystem, and the phonon scatterings between the two subsystems.

When the relaxation time approximation (RTA) is adopted for the phonon scatterings inside each subsystem, the Eq. (3-3a) and Eq. (3-3b) can be written as:

$$\mathbf{v}\cdot\nabla_{\mathbf{r}}f_1=\left(\frac{f_1-f_{1,0}}{\tau_{11}}\right)_{11}+\left(\frac{\partial f_1}{\partial t}\right)_{12} \tag{3-4a}$$

$$\mathbf{v}\cdot\nabla_{\mathbf{r}}f_2=\left(\frac{f_2-f_{2,0}}{\tau_{22}}\right)_{22}+\left(\frac{\partial f_2}{\partial t}\right)_{12} \tag{3-4b}$$

where $f_{1,0}$ and $f_{2,0}$ is the phonon distribution function inside the two subsystems at equilibrium (the Bose-Einstein distribution $f=(\exp(\hbar\omega/k_BT)-1)^{-1}$, respectively. τ_{11} and τ_{22} are the relaxation time for the phonons inside the two subsystems, respectively.

After multiplying Eq. (3-4a) and Eq. (3-4b) by $\hbar\omega$, and integrating over all wavevectors ($\mathbf{q}$), the first terms on the right-hand sides of Eq. (3-4a) and Eq. (3-4b) drop out because they are odd functions with respect to all wavevectors [44]. And they are described as:

$$\nabla_{\mathbf{r}}\cdot\sum_{\mathbf{q}}\hbar\omega_{\mathbf{q}}\mathbf{v}f_1=\sum_{\mathbf{q}}\hbar\omega_{\mathbf{q}}\left(\frac{\partial f_1}{\partial t}\right)_{12} \tag{3-5a}$$

$$\nabla_{\mathbf{r}}\cdot\sum_{\mathbf{q}}\hbar\omega_{\mathbf{q}}\mathbf{v}f_2=\sum_{\mathbf{q}}\hbar\omega_{\mathbf{q}}\left(\frac{\partial f_2}{\partial t}\right)_{12} \tag{3-5b}$$

Denoting $\mathbf{J}_{1/2}=\sum_{\mathbf{q}}\hbar\omega_{\mathbf{q}}\mathbf{v}f_{1/2}$ and $\partial E_{1/2}/\partial t=\sum_{\mathbf{q}}\hbar\omega_{\mathbf{q}}(\partial f_{1/2}/\partial t)_{12}$, then:

$$\nabla\cdot\mathbf{J}_1=-\frac{\partial E_1}{\partial t} \tag{3-6a}$$

$$\nabla\cdot\mathbf{J}_2=-\frac{\partial E_2}{\partial t} \tag{3-6b}$$

The phonon scatterings between the two subsystems are responsible for the local energy exchange between the two subsystems. When $1/\tau_{12}$ is used to describe the scattering rate for the coupling between the two subsystems, the rate of energy transfer between the two subsystems can be described by Ref. [45]:

$$\frac{\Delta E_1}{\Delta t}=\frac{c_1(T_{int}-T_1)}{\tau_{12}} \tag{3-7a}$$

$$\frac{\Delta E_2}{\Delta t}=\frac{c_2(T_{int}-T_2)}{\tau_{12}} \tag{3-7b}$$

$$T_{int}=\frac{c_1T_1+c_2T_2}{c_1+c_2} \tag{3-7c}$$

where c_1 (c_2) is the specific heat capacity of subsystem 1 (2), and T_{int}

is the intermediate temperature that both of the two subsystems approach.

Therefore, the rate of energy transfer is written as:

$$\frac{\Delta E_1}{\Delta t}=\frac{c_1c_2(T_2-T_1)}{\tau_{12}(c_1+c_2)}=G_c(T_2-T_1) \tag{3-8a}$$

$$\frac{\Delta E_2}{\Delta t}=\frac{c_1c_2(T_1-T_2)}{\tau_{12}(c_1+c_2)}=G_c(T_1-T_2) \tag{3-8b}$$

$$G_c=\frac{c_1c_2}{\tau_{12}(c_1+c_2)} \tag{3-8c}$$

where G_c is defined as the coupling factor. Then, with the heat diffusion equation, the Eq. (3-6a) and Eq. (3-6b) can be written as:

$$\nabla J_1=G_c(T_2-T_1) \tag{3-9a}$$

$$\nabla J_2=G_c(T_1-T_2) \tag{3-9b}$$

Then, the Fourier's definition, $J=-\kappa\nabla T$, is applied to rewrite the Eq. (3-9a) and Eq. (3-9b):

$$-\kappa_1\nabla^2T_1=G_c(T_2-T_1) \tag{3-10a}$$

$$-\kappa_2\nabla^2T_2=G_c(T_1-T_2) \tag{3-10b}$$

Considering the one-dimensional temperature gradient, the governing equations for coupled phonon transport states can be written as:

$$-\kappa_1\frac{d^2T_1}{dx^2}=G_c(T_2-T_1) \tag{3-11a}$$

$$-\kappa_2\frac{d^2T_2}{dx^2}=G_c(T_1-T_2) \tag{3-11b}$$

Subtracting Eq. (3-11a) from Eq. (3-11b), the temperature difference (θ) between the two subsystems can be described as:

$$\frac{d^2\theta}{dx^2}-\gamma^2\theta=0 \tag{3-12}$$

where $\theta=T_2-T_1$, and $\gamma=\sqrt{G_c(1/\kappa_1+1/\kappa_2)}$.

Based on the solution of Eq. (3-12), the temperature difference distribution is an exponential function of the position (x), and its detailed form depends on the corresponding boundary conditions in specific applications.

During the derivation of PWCM, it is worth noting that the coupling between two interacting subsystems is required to be so weak that it has a negligible effect on the distribution and phase space of phonons in two separate subsystems. Therefore, the requirement of weak coupling need be meet in applications of PWCM.

Here, PWCM is derived on the base of Boltzmann transport equation. It is worth to note that BTE is applicable to describe the physics under the particle picture, not include explicit wave effects [44]. So, BTE is not only applicable to diffusive transport, but also suitable for ballistic transport under certain conditions.

There is size effect in micro/nanoscale phonon transport when the size of structures is comparable to the mean free path of phonons. For classical size effects which do not consider quantum effect, the phonon transport is largely affected by boundary scatterings. Transport processes of classical size effects can be treated on the basis of BTE by treating phonons as particles [44].

Ma et al. quantified the contribution of phonon particle and wave effects in Si nanowires with a few nanometers in diameter [46]. It was found that the particle effect is quite significant as well and contributes 40% to the thermal conductivity reduction by nanopillars. Therefore, it can be seen that the particle characteristics of phonon transport still exist widely in the nanoscale materials.

Therefore, BTE is still applicable to describe a wide range of physical process at the micro/nano scale, as stated by Chen that "*Despite these restrictions, the Boltzmann equation is powerful and can be applied to a wide range of problems from nanoscale to macroscale*" [44].

Besides, in bulk materials, frequent collisions occur among phonons resulting in strong phonon-phonon couplings, which corresponds to the diffusive characteristic. However, for low-dimensional nanostructures, the size reaches nanoscale and a number of phonon modes are largely reduced. Quasi-ballistic transport is often present, which is easier to occur weaker phonon-phonon couplings. Therefore, composite of strong and weak couplings are presented in low dimensional materials. For example, in two-dimensional graphene, the coupling inside the in-/out-plane phonon groups is strong, while the coupling between them is weak. The PWCM is applicable to describe the composite couplings in low-dimensional materials, instead of strong couplings in bulk materials.

4. Applications of PWCM

Since the PWCM embodies the advantages of clear physical description of phonon weak coupling mechanism, it has some important applications for better understanding of coupled thermal transport in materials. Generally, the PWCM is applicable to two situations: one is "implicit couplings" describing couplings within a single structure, such as coupling between different phonon groups/branches; the other is "explicit couplings" describing couplings between two structures, such as interfacial thermal conductance between two different materials.

4.1. Implicit couplings

In low-dimensional materials, due to the obvious difference in properties between different phonon groups, there is weak couplings between different phonon groups which has non-negligible impact on the thermal properties. In the study of the previous work [22], the coupling mechanism between in-plane and out-of-plane phonon groups is revealed in nanosized graphene, a representative two-dimensional material with the highest known thermal conductivity [47,48]. As is shown in Fig. 2, the phonons in graphene are divided into two groups, namely in-plane (IP) group whose vibration direction is denoted by green arrow, and out-of-plane (OP) phonon group whose vibration direction is denoted by black arrow. In order to exhibit the coupling interaction, the temperature profile is shown in two different simulation regions with/without the coupling between IP and OP groups.

The PWCM can be applied here to illustrate the essential mechanism of coupling between different phonon groups. On the basis of the derivation of PWCM, the temperature difference distribution between OP and IP phonon group satisfies the function form of Eq. (3-12). According to the specific boundary condition $\theta|_{x\to-\infty}=0$ and $\theta|_{x=0}=\theta_{\max}$, the temperature difference distribution function is written as:

$$\theta=\theta_{\max}\exp(\gamma x) \tag{4-1}$$

The corresponding temperature difference profile is shown in

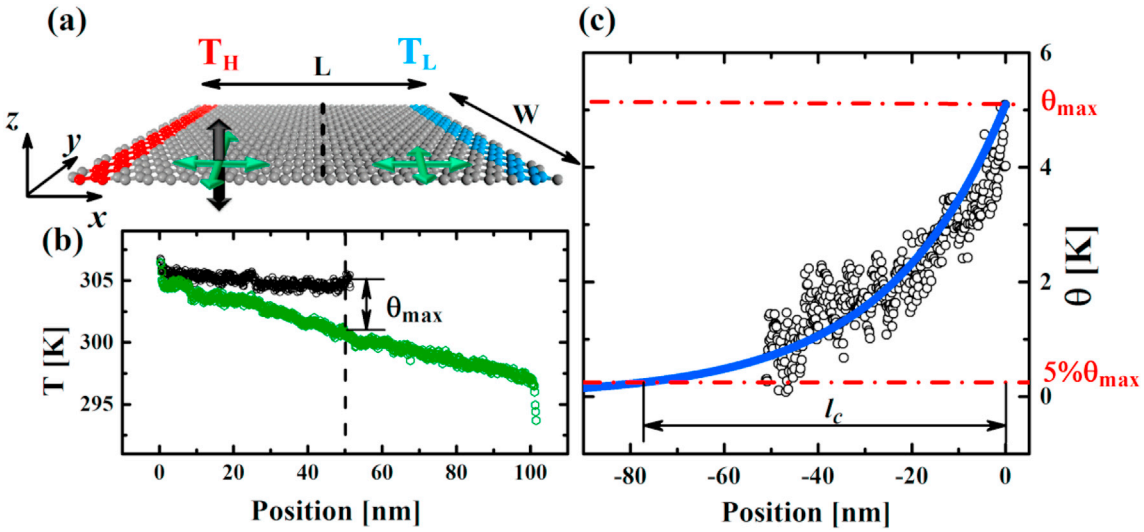

Fig. 2. Illustration of the weak coupling between in-plane (IP) and out-of-plane (OP) phonon groups in nanosized graphene from Ref. [22]. (a) Schematic illustration of molecular dynamics simulation setup. The black (green) arrow denotes the vibration along the OP (IP) direction. (b) The temperature profile of different phonon groups, where the black color is for OP phonon groups and the green color is for IP phonon groups. (c) The temperature difference distribution between OP and IP phonon groups. Reprinted with permission from Ref. [22]. Copyright (2017) American Chemical Society.

Fig. 2(c), and the distribution function is further verified by MD simulation in the work of Ref. [22].

In this application for coupled phonon transport in graphene, the phonon-phonon coupling factor (G_{io}) and coupling length (l_c) are given to characterize the coupling effect quantitatively, as given in Eq. (4-2) and Eq. (4-3). It is worth noting that the IP-OP coupling factor (G_{io}) is a representative form of the coupling factor (G_c) in the PWCM, and G_{io} is found not sensitive to system size. Besides, the physical meaning of coupling length (l_c) is the distance required to equilibrate OP and IP phonon groups when the temperature difference exists, which is denoted by the distance between the position of θ_{max} and $5\%\theta_{max}$ as given below:

$$G_{io} = \frac{c_i c_o}{\tau_{io}(c_i + c_o)} \tag{4-2}$$

$$l_c = \frac{-\ln(5\%)}{\gamma} \approx \frac{3}{\gamma} = \frac{3}{\sqrt{G_{io}\left(\frac{1}{\kappa_i} + \frac{1}{\kappa_o}\right)}} \tag{4-3}$$

This application of PWCM successfully demonstrates the weak coupling between IP and OP phonon groups in nanosized graphene [49–52]. Both the experimental and simulation work [53,54] have implied the coupling of IP-OP is much weaker than that of either IP-IP or OP-OP. It is deemed that the IP-OP coupling has a negligible effect on the distribution and phase space of either IP or OP phonon group. Therefore, the IP-OP coupling satisfies the premise of PWCM. Therefore, the PWCM can be successfully applied to illustrate the coupled thermal transport mechanism inside low-dimensional materials, and clearly predict and explain the thermal property of single material itself.

On the other hand, the PWCM can be also applied to reveal the non-equilibrium characteristic between different phonon branches or phonon modes, which is similar to the two-temperature model used in previous works. Ruan et al. has carried out a series of constructive works on non-equilibrium phonon transport [43,55,56]. They developed a spectral phonon temperature (SPT) method which could calculate the temperatures of phonons in both real and phase spaces within the framework of molecular dynamics [43]. The local non-equilibrium between the ballistic and diffusive phonons was observed both in nanomaterials such as silicon thin film and graphene, and cross interfaces such as graphene-graphene junction and graphene-boron nitride planar. It was found that, in the dimensionally mismatched interfaces, the couplings between the acoustic phonon modes are strong on both sides but become weaker with interfacial mixing, which introduces a new mechanism of thermal interfacial resistance. Also, the interface roughness is found to affect the coupling and non-equilibrium and shift the thermal transport channel.

Moreover, a multi-temperature model (MTM) method was proposed by Ruan et al. to capture the coupling between interfacial and bulk thermal transports, which presents phonon non-equilibrium thermal transport process at the Si-Ge interface [55]. As is shown in Fig. 3, the temperatures of different phonon branches deviate from each other near the interface, which presents the thermal non-equilibrium due to energy re-distribution caused by different thermal properties and transmission coefficients across the interface. The phonon branch-resolved temperature profile was predicted by MTM, and the coupling strengths between phonon branches were determined by using the relaxation time approximation. The non-equilibrium transport near the interface resulted in an additional thermal resistance, which caused that the overall interfacial thermal conductance of Si-Ge interface using MTM was 5.4% smaller than the conventional prediction. It is worth mentioning that non-equilibrium phonon transport is not very significant at Si-Ge interface, which indicates that the phonon-phonon coupling induced by Si-Ge interface is not very weak.

Besides, Ruan et al. developed a modal non-equilibrium molecular dynamics simulations to study the Si-Ge interfacial thermal transport and modified the Landauer approach to include the inelastic transmission and modal thermal non-equilibrium [56]. It was found that phonon modes were in strong thermal non-equilibrium near the interface, where optical phonon modes could contribute equal or more thermal conductance than the acoustic modes due to the bridging effect. The existence of the interfacial modes' bridging effect could boost the inelastic transport and even create effective four-phonon processes to help the transmission of high-frequency phonons.

Additionally, from the view of experimental research, Sullivan

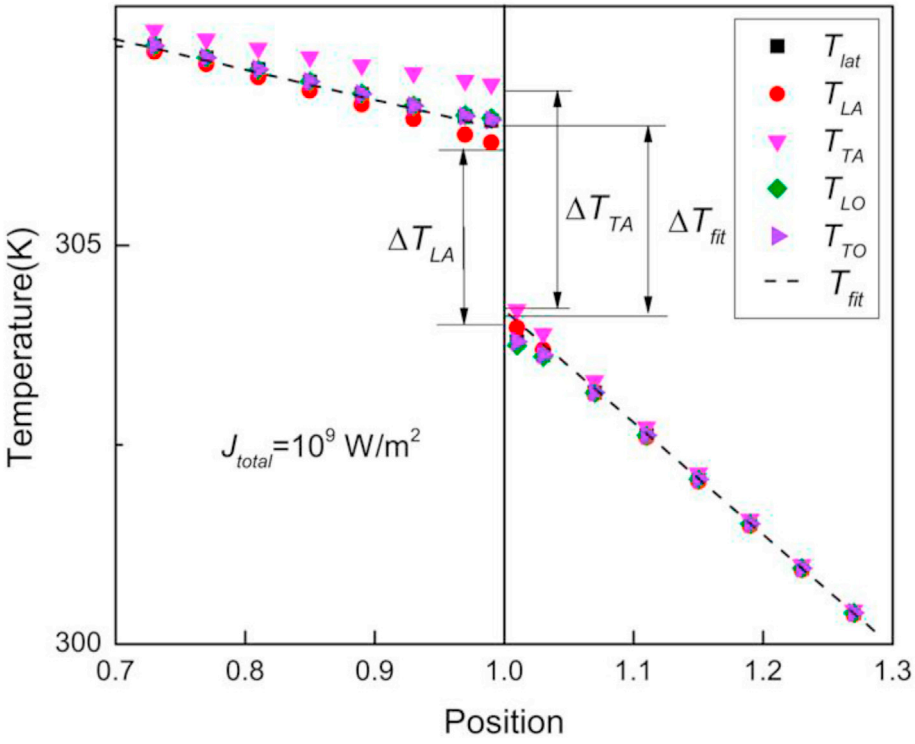

Fig. 3. Temperature profile predicted by MTM across a Si-Ge interface from Ref. [55]. Due to different interfacial transmission coefficients, the temperatures of different phonon branches (LA, TA, LO, TO) present some deviation from each other near the interface. Phonon-phonon couplings cause the thermal non-equilibrium which results in the decrease of interfacial conductance. Reprinted with permission from Ref. [55]. Copyright (2019) AIP Publishing.

et al. measured the temperatures of different phonon modes in a single layer of suspended graphene by Raman method, and found that there was a large temperature difference between different phonon modes which resulted in the non-equilibrium phonon transport [42]. The experimental finding revealed the weak coupling between optical phonons and different acoustic phonon polarizations. The observed local non-equilibrium phonon transport phenomena would have important implications for understanding energy dissipation mechanism in graphene-based electronic and optoelectronic devices.

4.2. Explicit couplings

From the derivation of PWCM, there is a particle conduction term in the space domain which allows the calculation of analytical solution for the spatial temperature profiles. Hence, the PWCM becomes an effective tool in the applications of studying the coupling of different thermal transport channels across the interfaces between different structures or materials.

There is a large number of nanoscale van der Waals interfaces in the microelectronics, photonics, and thermoelectric devices. A deep understanding of thermal transport through van der Waals interfaces is crucial to improve the performance of materials and devices for effective heat dissipation. For widespread van der Waals interfaces between two overlapped low-dimensional structures (that is vdW cross-interfaces), the heat flows along the structure horizontally and through the interface vertically simultaneously. It is obvious that the thermal transport at the vdW cross-interfaces is a two-dimensional process, which is different from the one-dimensional thermal transport of ordinary interfaces [58–60,70]. Thus, some traditional approximation methods like point contact treatment are not reasonable and lack the exploration for the essential mechanism to clearly describe the thermal transport at the vdW cross-interfaces [61,62]. Here, the PWCM is applicable to illustrate the two-dimensional thermal transport process at the vdW cross-interfaces by considering the coupling between different thermal transport channels.

In the previous work [63], an analytical model named as cross-interface model (CIM) which is essentially based on PWCM, is proposed to reveal the thermal transport mechanism at the vdW cross-interface between two structures with different thermal conductivities. The coupling between different thermal transport channels reasonably exhibits the two-dimensional process of thermal transport at the vdW cross-interfaces.

As is shown in Fig. 4(a), a vdW cross-interface is schematically represented by two ribbons with an overlapped region. Here, the two ribbons are assumed to have different thermal conductivities (κ_1 and κ_2) and cross section areas (A_1 and A_2) for universal applicability. Heat source and sink are imposed on the end of top and bottom ribbon respectively. On the basis of Eq. (3-11a) and Eq. (3-11b) for coupled phonon transport states in previous derivation of PWCM, the steady-state heat conduction in the two overlapped ribbons can be described as:

$$\kappa_1 \frac{d^2 T_T}{dx^2} A_1 - G_{CA}(T_T - T_B)w = 0, 0 < x < L_C \tag{4-4a}$$

$$\kappa_2 \frac{d^2 T_B}{dx^2} A_2 + G_{CA}(T_T - T_B)w = 0, 0 < x < L_C \tag{4-4b}$$

The above governing equations also satisfy the general Fourier' law and energy conservation. Here, the interfacial thermal conductance (G_{CA}) can be considered as a kind of coupling factor (G_c) in PWCM, which characterizes the coupling effects between two-dimensional heat flow process in two overlapped channels. By combining Eq. (4-4a) and Eq. (4-4b), the following equations can be

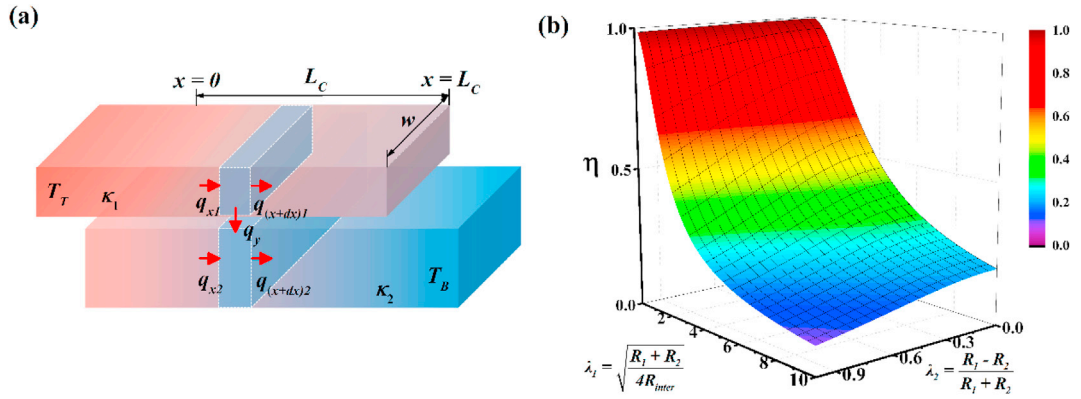

Fig. 4. Application of PWCM in the vdW cross-interface between two structures with different thermal conductivities from Ref. [63]. (a) Schematic diagram of vdW cross-interface model. (b) The dimensionless factor η in the expression of the total thermal resistance as a function of two influencing parameters, λ_1 and λ_2. Reprinted from Ref. [63] with permission from the PCCP Owner Societies. Copyright (2019) Royal Society of Chemistry.

obtained:

$$\frac{d^2(T_T - T_B)}{dx^2} = \gamma_1^2(T_T - T_B), 0 < x < L_C \tag{4-5a}$$

$$\frac{d^2(T_T + T_B)}{dx^2} = \gamma_2(T_T - T_B), 0 < x < L_C \tag{4-5b}$$

where, T_T and T_B denote the temperatures of top and bottom ribbons, respectively. $\gamma_1 = \sqrt{G_{CA}w/\kappa_1 A_1 + G_{CA}w/\kappa_2 A_2}$, $\gamma_2 = G_{CA}w/\kappa_1 A_1 - G_{CA}w/\kappa_2 A_2$.

Through a series of theoretical derivation, the total thermal resistance (R_{total}) in the system is expressed as:

$$R_{total} = \frac{L_C}{\kappa_1 A_1 + \kappa_2 A_2} + \frac{1}{\eta} \times \frac{1}{G_{CA}wL_C} = \frac{R_1 R_2}{R_1 + R_2} + \frac{1}{\eta} \times R_{inter} = R_{intra} + \frac{1}{\eta} \times R_{inter} \tag{4-6}$$

$$R_1 = \frac{L_C}{\kappa_1 A_1}, R_2 = \frac{L_C}{\kappa_2 A_2}, R_{intra} = \frac{R_1 R_2}{R_1 + R_2}, R_{inter} = \frac{1}{G_{CA}wL_C} \tag{4-6a}$$

$$\eta = \frac{1}{\lambda_1(\lambda_2 \tanh \lambda_1 + \coth \lambda_1)}, \lambda_1 = \sqrt{\frac{R_1 + R_2}{4R_{inter}}}, \lambda_2 = \frac{R_1 - R_2}{R_1 + R_2} \tag{4-6b}$$

From the analytical results, the total thermal resistance (R_{total}) is an organic combination of the intra-ribbon and inter-ribbon thermal resistance (R_{intra} and R_{inter}). In traditional approximation methods, the total thermal resistance is simply the sum of R_{intra} and R_{inter}, which is similar to the series law of electrical resistance [64]. However, the existence of dimensionless factor (η) in Eq. (4-6) reveals the essential coupling relationship between the intra-ribbon and inter-ribbon thermal transport, which exactly exhibits the advantage of the PWCM. Furthermore, the applicability of PWCM is validated through the comparison of the analytical results with MD simulations for a typical vdW cross-interface of two overlapped boron nitride nanoribbons in the work of Ref. [63].

On the other hand, the application of PWCM for vdW cross-interfaces can be extended to assist experimental measurement and explain theoretically the experimental results. The interfacial thermal conductance across nanoscale van der Waals interfaces remains poorly characterized in experiments because of technical challenges. In the previous work [65], the PWCM as an interfacial thermal transport model is combined with an experimental approach to determine the interfacial thermal conductance (G_{CA}) between two individual copper phthalocyanine (CuPc) nanoribbons, and analyze the related influencing factors on the interfacial thermal transport.

As is shown in Fig. 5(a), two CuPc nanoribbons with a planar contact bridges the suspended membranes of the measurement device for the measurement by thermal bridge method [66,67]. Such interfaces in experiments can be abstracted into a theoretical model as shown in Fig. 5(b), that is a vdW cross-interface between two parallel aligned nanoribbons with an overlap length L_C. Two nanoribbons are assumed to have the same width (w), thickness (t) and thermal conductivity (κ) since they are cut from the same CuPc nanoribbon. This theoretical model is essentially the same as the previous model shown in Fig. 4(a), and the only difference is that the thermal conductivity of the two structures is the same. Therefore, similar to Eq. (4-4a) and Eq. (4-4b), the steady-state heat conduction equations for top and bottom nanoribbons can be written as:

$$\kappa \frac{d^2T_T}{dx^2} wtdx - G_{CA}(T_T - T_B)wdx = 0 \tag{4-7a}$$

$$\kappa \frac{d^2T_B}{dx^2} wtdx + G_{CA}(T_T - T_B)wdx = 0 \tag{4-7b}$$

Since the heat rate (q) can be calculated by integrating the heat flux over the interface, the thermal resistance of the overlapped region between two nanoribbons (R_{CC}) can be derived as:

$$R_{CC} = \frac{T_T|_{-L_C/2} - T_B|_{L_C/2}}{q} = \frac{L_C}{2\kappa wt} + \frac{1}{\eta}\frac{1}{wL_C G_{CA}} == R_{intra} + \frac{1}{\eta}R_{inter} \tag{4-8}$$

$$R_{intra} = \frac{L_C}{2\kappa wt}, R_{inter} = \frac{1}{G_{CA}wL_C}, \eta = \tanh\left(\frac{\gamma L_C}{2}\right)\Big/\frac{\gamma L_C}{2}, \frac{\gamma L_C}{2} = \sqrt{\frac{R_{intra}}{R_{inter}}} \tag{4-8a}$$

Here, the thermal resistance (R_{CC}) is a special form of the previous thermal resistance (R_{total}) in Eq. (4-6) for the situations of two overlapped structures with the same thermal conductivity.

In the experimental measurement, the temperature, thermal

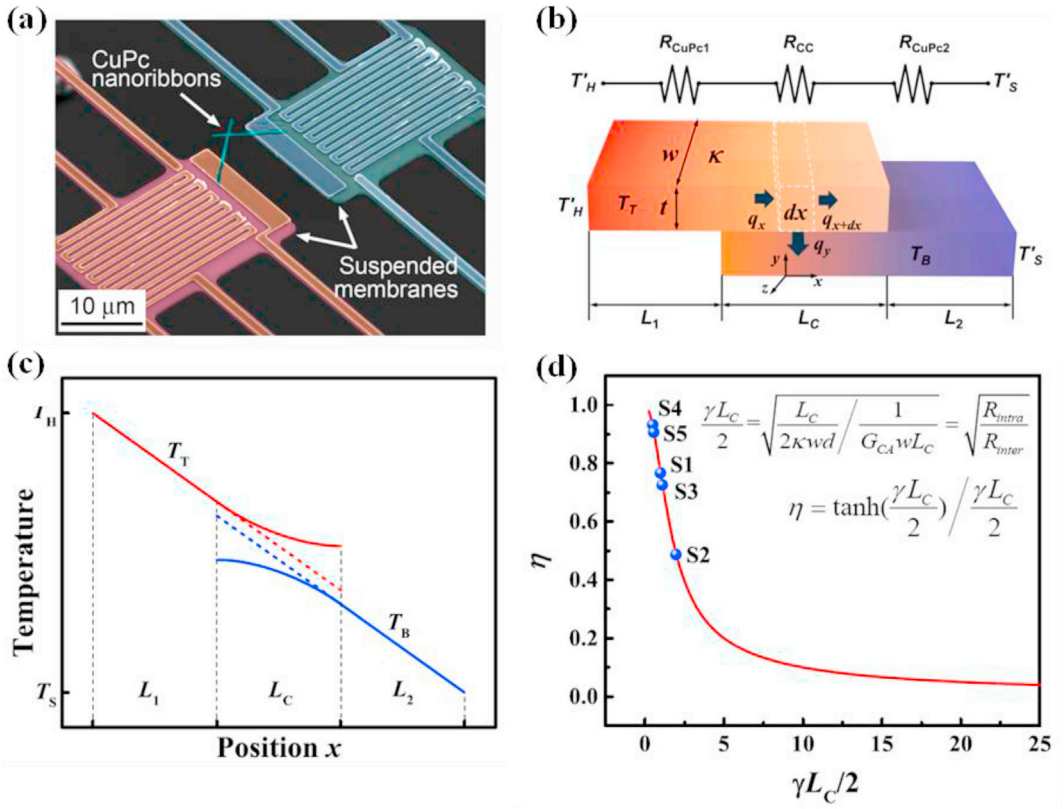

Fig. 5. Application of PWCM in thermal transport through the van der Waals interface between two individual CuPc nanoribbons from Ref. [65]. (a) False-color SEM micrograph of two CuPc nanoribbons with a planar contact on a suspended device for thermal measurement. (b) Schematic of two overlapped nanoribbons and the corresponding thermal circuit. (c) The temperature distribution profiles of top and bottom nanoribbons. (d) The dimensionless factor (η) as a function of characteristic parameter ($\frac{\gamma L_C}{2}$). Adapted with permission from Ref. [65]. Copyright (2019) Elsevier.

conductivity and geometric parameters of both structures can be obtained, so the interfacial thermal conductance (G_{CA}) can be determined by solving Eq. (4-8). If adopting traditional approximation approach [61], the thermal resistance of the overlapped region can be expressed as:

$$R_{CC,app} = \frac{L_C}{\kappa wt} + \frac{1}{wL_C G_{CA}} = R_{intra} + R_{inter} \tag{4-9}$$

The only difference between the analytical model based on PWCM and approximate model is the existence of dimensionless factor (η), which is due to the nonlinear temperature distribution caused by the coupled thermal transport across the interface. Fig. 5(c) shows the temperature distribution of the upper and lower nanoribbons. The temperature distribution in the non-overlapped region is linear, while that in the overlapped region is nonlinear so the temperature difference does not keep constant. However, in the approximate model, the temperature difference between two overlapped ribbons is considered constant [61].

The dimensionless factor (η) can be considered as the heat coupling efficiency of vdW cross-interfaces. Fig. 5(d) plots the factor (η) as a function of characteristic parameter ($\frac{\gamma L_C}{2}$), which indicates the relative ratio of R_{intra} and R_{inter}. When $\frac{\gamma L_C}{2} = 0$ (corresponding to $R_{intra} \ll R_{inter}$), the factor (η) is equal to 1, indicating that the analytical model coincides with the approximation approach. However, for CuPc nanoribbons with relatively large intrinsic thermal resistances, the factor (η) will be less than 1, even as small as 0.48 shown by the blue dots for experimental samples. Thus the analytical model based on PWCM is more appropriate to determine the interfacial thermal conductance (G_{CA}), while the approximation approach will overestimate the G_{CA}. Therefore, the application of the PWCM theoretical model is able to reasonably elucidate the fundamental mechanisms for the ultralow interfacial thermal conductance observed in practical experiment measurement.

5. Summary and outlook

In this work, on the basis of reviewing recent studies on weak couplings between phonon and other energy carriers, a generalized analytical model named phonon weak couplings model, is proposed based on Boltzmann transport equation to reveal the phonon-phonon weak coupling mechanism for thermal transport. The applications of PWCM to describe recent works on phonon couplings, are classified and demonstrated in two situations: one is “implicit couplings” between different phonon groups/branches within the single structure, the other is “explicit couplings” across the vdW cross-interface between two different structures. The merit of this work lies in the fact that the essential mechanism of phonon weak couplings is explored theoretically, and the proposed generalized model is applied in both the single materials itself and the composite materials with interfaces in a systematic way. Besides, on the basic framework of PWCM, some physical parameters are excavated to characterize the coupling effect quantitatively, such as the phonon-phonon coupling factor (G_{io}) and coupling length (l_c) for the coupled phonon transport inside low-dimensional materials, and the interfacial thermal conductance (G_{CA}) and dimensionless factor (η) for the coupled thermal transport at the vdW cross-interfaces. Thus, PWCM not only provides a new perspective to deepen the understanding of coupled thermal

transport, but also explores feasible methods to improve the thermal performance for effective thermal management.

The phonon weak couplings are not just limited to thermal management, but also make the possibility of phonon quantum modulation, that is, adjusting a few key eigen modes in modulation. For example, Kiarash et al. utilized the characteristics of phonon weak coupling to create a type of "phonon catalysis", whereby only a few phonon modes that matter most are targeted and deliberately excited to accelerate a chemical reaction [69]. Thus, the speed of chemical transformations can be controlled through phonons/atomic vibrations, instead of traditional electronic structure, which represents a major advance that has far reaching implications that could spark the creation of an entirely new field. In addition, by using a stimulus such as light (photons) or electrons to selectively excite certain targeted phonon eigen modes, it is likely to make a material exhibit extremely fast kinetics associated with an extremely local high temperature, while the bulk temperature of material remains much lower. This could provide a new avenue for energy storage technology.

Still, the limitations of PWCM should not be overlooked. PWCM selects the Fourier's definition of thermal conductivity which is independent on size and valid in macroscopic. It is acceptable for micro/nano structures with ultra-low thermal conductivity and short phonon mean free path. For the other nanostructures having size-dependent thermal conductivity, the phonon coupling mechanism needs further deep-going investigation. It is worth noting that, even though there is size effect in nanostructure, when the size of nanostructure is fixed, the thermal conductivity still keeps constant which could also use PWCM to analyze the coupling effect. Additionally, in applications of PWCM, it requires that the couplings between the two subsystems should be much weaker than those inside each subsystem. However, it is difficult to quantitatively describe the relationship. These limitations and potential research aspirations deserve further investigations in the future.

Declaration of competing interest

The authors declare that they have no known competing financial interests or personal relationships that could have appeared to influence the work reported in this paper.

Acknowledgement

This work was financially supported by the National Natural Science Foundation of China No. 51606072 (CD), National Key Research and Development Project of China No. 2018YFE0127800 (NY), and Natural Science Foundation of Shaanxi Province No. 2020JQ-629 (MA).

References

[1] D.G. Cahill, P.V. Braun, C. Gang, D.R. Clarke, L. Shi, Nanoscale thermal transport. II. 2003–2012, Appl. Phys. Rev. 1 (2014) 011305.
[2] X. Xu, J. Chen, J. Zhou, B. Li, Thermal conductivity of polymers and their nanocomposites, Adv. Mater. 30 (2018) 1705544.
[3] J. Hansson, T.M.J. Nilsson, L. Ye, J. Liu, Novel nanostructured thermal interface materials: a review, Int. Mater. Rev. 63 (2017) 22–45.
[4] K.M. Razeeb, E. Dalton, G.L.W. Cross, A.J. Robinson, Present and future thermal interface materials for electronic devices, Int. Mater. Rev. 1 (2018) 1–21.
[5] A. Bar-Cohen, K. Matin, S. Narumanchi, Nanothermal interface materials: technology review and recent results, J. Electron. Packag. 137 (2015): 040803.
[6] P.M. Norris, N.Q. Le, C.H. Baker, Tuning phonon transport: from interfaces to nanostructures, J. Heat Tran. 135 (2013).
[7] S. Volz, J. Shiomi, M. Nomura, K. Miyazaki, Heat conduction in nanostructured materials, J. Therm. Sci. Technol. 11 (2016). JTST0001.
[8] N. Li, J. Ren, L. Wang, G. Zhang, P. Hänggi, B. Li, Colloquium: phononics: Manipulating heat flow with electronic analogs and beyond, Rev. Mod. Phys. 84 (2012) 1045–1066.
[9] X. Gu, Y. Wei, X. Yin, B. Li, R. Yang, Colloquium: phononic thermal properties of two-dimensional materials, Rev. Mod. Phys. 90 (2018) 041002.
[10] N. Yang, X. Xu, G. Zhang, B. Li, Thermal transport in nanostructures, AIP Adv. 2 (2012) 041410.
[11] M. Maldovan, Sound and heat revolutions in phononics, Nature 503 (2013) 209–217.
[12] Y. Xiao, Q. Chen, D. Ma, N. Yang, Q. Hao, Phonon transport within periodic porous structures – from classical phonon size effects to wave effects, ES Mater. Manuf. 5 (2019) 2–18.
[13] X. Wu, T. Luo, The importance of anharmonicity in thermal transport across solid-solid interfaces, J. Appl. Phys. 115 (2014) 014901.
[14] K.M. Shahil, A.A. Balandin, Graphene–multilayer graphene nanocomposites as highly efficient thermal interface materials, Nano Lett. 12 (2012) 861–867.
[15] K.M.F. Shahil, A.A. Balandin, Thermal properties of graphene and multilayer graphene: applications in thermal interface materials, Solid State Commun. 152 (2012) 1331–1340.
[16] A.A. Balandin, S. Ghosh, W. Bao, I. Calizo, D. Teweldebrhan, F. Miao, C.N. Lau, Superior thermal conductivity of single-layer graphene, Nano Lett. 8 (2008) 902–907.
[17] V. Sharma, H.L. Kagdada, P.K. Jha, P. Spiewak, K.J. Kurzydowski, Thermal transport properties of boron nitride based materials: a review, Renew. Sustain. Energy Rev. 120 (2020) 109622.
[18] J. Ordonez-Miranda, J.J. Alvarado-Gil, R. Yang, The effect of the electron-phonon coupling on the effective thermal conductivity of metal-nonmetal multilayers, J. Appl. Phys. 109 (2011) 094310.
[19] N. Yang, X. Ni, J.-W. Jiang, B. Li, How does folding modulate thermal conductivity of graphene? Appl. Phys. Lett. 100 (2012) 093107.
[20] G. Peng, H. Ding, S.W. Sharshir, X. Li, H. Liu, D. Ma, L. Wu, J. Zang, H. Liu, W. Yu, H. Xie, N. Yang, Low-cost high-efficiency solar steam generator by combining thin film evaporation and heat localization: both experimental and theoretical study, Appl. Therm. Eng. 143 (2018) 1079–1084.
[21] X. Li, G. Xu, G. Peng, N. Yang, W. Yu, C. Deng, Efficiency enhancement on the solar steam generation by wick materials with wrapped graphene nanoparticles, Appl. Therm. Eng. 161 (2019) 114195.
[22] M. An, Q. Song, X. Yu, H. Meng, D. Ma, R. Li, Z. Jin, B. Huang, N. Yang, Generalized two-temperature model for coupled phonons in nanosized graphene, Nano Lett. 17 (2017) 5805–5810.
[23] L. Beguin, A. Vernier, R. Chicireanu, T. Lahaye, A. Browaeys, Direct measurement of the van der Waals interaction between two Rydberg atoms, Phys. Rev. Lett. 110 (2013) 263201.
[24] L.M. Woods, D.A.R. Dalvit, A. Tkatchenko, P. Rodriguez-Lopez, A.W. Rodriguez, R. Podgornik, Materials perspective on Casimir and van der Waals interactions, Rev. Mod. Phys. 88 (2016) 045003.
[25] S. Ghosh, W. Bao, D.L. Nika, S. Subrina, E.P. Pokatilov, C. Ning Lau, A.A. Balandin, Dimensional crossover of thermal transport in few-layer graphene, Nat. Mater. 9 (2010) 555–558.
[26] Z. Lu, X. Ruan, Non-equilibrium thermal transport: a review of applications and simulation approaches, ES Energy Environ. 4 (2019) 5–14.
[27] D.J. Sanders, D. Walton, Effect of magnon-phonon thermal relaxation on heat transport by magnons, Phys. Rev. B 15 (1977) 1489–1494.
[28] A. Majumdar, P. Reddy, Role of electron–phonon coupling in thermal conductance of metal–nonmetal interfaces, Appl. Phys. Lett. 84 (2004) 4768–4770.
[29] S.I. Anisimov, B.L. Kapeliovich, T.L. Perel'Man, Electron emission from metal surfaces exposed to ultrashort laser pulses, Soviet J. Exp. Theor. Phys. 39 (1974) 375.
[30] G. Chen, Potential-step amplified nonequilibrium thermal-electric converters, J. Appl. Phys. 97 (2005) 083707.
[31] N. Yang, T. Luo, K. Esfarjani, A. Henry, Z. Tian, J. Shiomi, Y. Chalopin, B. Li, G. Chen, Thermal interface conductance between aluminum and silicon by molecular dynamics simulations, J. Comput. Theor. Nanosci. 12 (2015) 168–174.
[32] Y. Wang, X. Ruan, A.K. Roy, Two-temperature nonequilibrium molecular dynamics simulation of thermal transport across metal-nonmetal interfaces, Phys. Rev. B 85 (2012) 205311.
[33] Z. Lu, Y. Wang, X. Ruan, Metal/dielectric thermal interfacial transport considering cross-interface electron-phonon coupling: theory, two-temperature molecular dynamics, and thermal circuit, Phys. Rev. B 93 (2016) 064302.
[34] A.K. Vallabhaneni, D. Singh, H. Bao, J. Murthy, X. Ruan, Reliability of Raman measurements of thermal conductivity of single-layer graphene due to selective electron-phonon coupling: a first-principles study, Phys. Rev. B 93 (2016): 125432.
[35] Z. Lu, A. Vallabhaneni, B. Cao, X. Ruan, Phonon branch-resolved electron-phonon coupling and the multitemperature model, Phys. Rev. B 98 (2018) 134309.
[36] Y. Wang, Z. Lu, A.K. Roy, X. Ruan, Effect of interlayer on interfacial thermal transport and hot electron cooling in metal-dielectric systems: an electron-phonon coupling perspective, J. Appl. Phys. 119 (2016) 065103.
[37] Z. Lu, Y. Wang, X. Ruan, The critical particle size for enhancing thermal conductivity in metal nanoparticle-polymer composites, J. Appl. Phys. 123 (2018) 074302.
[38] J. Xiao, G.E.W. Bauer, K.-C. Uchida, E. Saitoh, S. Maekawa, Theory of magnon-driven spin Seebeck effect, Phys. Rev. B 81 (2010) 214418.
[39] M. Schreier, A. Kamra, M. Weiler, J. Xiao, G.E.W. Bauer, R. Gross, S.T.B. Goennenwein, Magnon, phonon, and electron temperature profiles and

the spin Seebeck effect in magnetic insulator/normal metal hybrid structures, Phys. Rev. B 88 (2013) 094410.
[40] B. Liao, J. Zhou, G. Chen, Generalized two-temperature model for coupled phonon-magnon diffusion, Phys. Rev. Lett. 113 (2014) 025902.
[41] K. An, K.S. Olsson, A. Weathers, S. Sullivan, X. Chen, X. Li, L.G. Marshall, X. Ma, N. Klimovich, J. Zhou, L. Shi, Magnons and phonons optically driven out of local equilibrium in a magnetic insulator, Phys. Rev. Lett. 117 (2016) 107202.
[42] S. Sullivan, A. Vallabhaneni, I. Kholmanov, X. Ruan, J. Murthy, L. Shi, Optical generation and detection of local nonequilibrium phonons in suspended graphene, Nano Lett. 17 (2017) 2049–2056.
[43] T. Feng, W. Yao, Z. Wang, J. Shi, C. Li, B. Cao, X. Ruan, Spectral analysis of nonequilibrium molecular dynamics: spectral phonon temperature and local nonequilibrium in thin films and across interfaces, Phys. Rev. B 95 (2017) 195202.
[44] G. Chen, Nanoscale Energy Transport and Conversion: a Parallel Treatment of Electrons, Molecules, Phonons, and Photons, Oxford University Press, 2005, p. 282.
[45] D. Sanders, D. Walton, Effect of magnon-phonon thermal relaxation on heat transport by magnons, Phys. Rev. B 15 (1977) 1489.
[46] D. Ma, A. Arora, S. Deng, G. Xie, J. Shiomi, N. Yang, Quantifying phonon particle and wave transport in silicon nanophononic metamaterial with cross junction, Mater. Today Phys. 8 (2019) 56–61.
[47] X. Xu, L.F. Pereira, Y. Wang, J. Wu, K. Zhang, X. Zhao, S. Bae, C. Tinh Bui, R. Xie, J.T. Thong, B.H. Hong, K.P. Loh, D. Donadio, B. Li, B. Ozyilmaz, Length-dependent thermal conductivity in suspended single-layer graphene, Nat. Commun. 5 (2014) 3689.
[48] A.A. Balandin, S. Ghosh, W. Bao, I. Calizo, D. Teweldebrhan, F. Miao, C.N. Lau, Superior thermal conductivity of single-layer graphene, Nano Lett. 8 (2008) 902–907.
[49] J. Zhang, Y. Wang, X. Wang, Rough contact is not always bad for interfacial energy coupling, Nanoscale 5 (2013) 11598–11603.
[50] J. Zhang, X. Wang, H. Xie, Co-existing heat currents in opposite directions in graphene nanoribbons, Phys. Lett. A 377 (2013) 2970–2978.
[51] J. Zhang, X. Huang, Y. Yue, J. Wang, X. Wang, Dynamic response of graphene to thermal impulse, Phys. Rev. B 84 (2011) 235416.
[52] H. Zhang, G. Lee, K. Cho, Thermal transport in graphene and effects of vacancy defects, Phys. Rev. B 84 (2011) 115460.
[53] S. Sullivan, A. Vallabhaneni, I. Kholmanov, X. Ruan, J. Murthy, L. Shi, Optical generation and detection of local nonequilibrium phonons in suspended graphene, Nano Lett. 17 (2017) 2049–2056.
[54] A.K. Vallabhaneni, D. Singh, H. Bao, J. Murthy, X. Ruan, Reliability of Raman measurements of thermal conductivity of single-layer graphene due to selective electron-phonon coupling: a first-principles study, Phys. Rev. B 93 (2016) 125432.
[55] Z. Lu, J. Shi, X. Ruan, Role of phonon coupling and non-equilibrium near the interface to interfacial thermal resistance: the multi-temperature model and thermal circuit, J. Appl. Phys. 125 (2019) 085107.
[56] T. Feng, Y. Zhong, J. Shi, X. Ruan, Unexpected high inelastic phonon transport across solid-solid interface: modal nonequilibrium molecular dynamics simulations and Landauer analysis, Phys. Rev. B 99 (2019): 045301.
[58] H. Zhang, S. Xiong, H. Wang, S. Volz, Y. Ni, Thermal transport in graphene/h-BN lateral heterostructures with interface compositional diffusion, Europhys. Lett. 125 (2019) 46001.
[59] Z. Tian, K. Esfarjani, G. Chen, Enhancing phonon transmission across a Si/Ge interface by atomic roughness: first-principles study with the Green's function method, Phys. Rev. B 86 (2012) 235304.
[60] Y. Yang, H. Chen, H. Wang, N. Li, L. Zhang, Optimal thermal rectification of heterojunctions under Fourier law, Phys. Rev. E 98 (2018): 042131.
[61] J. Yang, S. Waltermire, Y. Chen, A.A. Zinn, T.T. Xu, D. Li, Contact thermal resistance between individual multiwall carbon nanotubes, Appl. Phys. Lett. 96 (2010) 023109.
[62] X. Liu, G. Zhang, Y.W. Zhang, Thermal conduction across graphene cross-linkers, J. Phys. Chem. C 118 (2014) 12541–12547.
[63] W. Feng, X. Yu, Y. Wang, D. Ma, Z. Sun, C. Deng, N. Yang, A cross-interface model for thermal transport across the interface between overlapped nanoribbons, Phys. Chem. Chem. Phys. 21 (2019) 25072–25079.
[64] J. Yang, S. Waltermire, Y. Chen, A.A. Zinn, T.T. Xu, D. Li, Contact thermal resistance between individual multiwall carbon nanotubes, Appl. Phys. Lett. 96 (2010) 630.
[65] Y. Xiong, X. Yu, Y. Huang, J. Yang, L. Li, N. Yang, D. Xu, Ultralow thermal conductance of the van der Waals interface between organic nanoribbons, Mater. Today Phys. 11 (2019) 100139.
[66] H. Tang, X.M. Wang, Y.C. Xiong, Y. Zhao, Y. Zhang, Y. Zhang, J.K. Yang, D.Y. Xu, Thermoelectric characterization of individual bismuth selenide topological insulator nanoribbons, Nanoscale 7 (2015) 6683–6690.
[67] L. Shi, D.Y. Li, C.H. Yu, W.Y. Jang, D. Kim, Z. Yao, P. Kim, A. Majumdar, Measuring thermal and thermoelectric properties of one-dimensional nanostructures using a microfabricated device, J. Heat Transf. 125 (2003) 881–888.
[69] G. Kiarash, S. Muy, S.-H. Yang, H. Asegun, Enhancement of ion diffusion by targeted phonon excitation, in: ECS Meeting, 2020. MA2020-01(1):96-96.
[70] S. Ju, T. Shiga, L. Feng, Z. Hou, K. Tsuda, J. Shiomi, Designing nanostructures for phonon transport via Bayesian optimization, Phys. Rev. X 7 (2017) 021024.